The International Journal of Advanced Manufacturing Technology
https://doi.org/10.1007/s00170-026-18114-5

ORIGINAL ARTICLE

An improved upcycling approach for producing bimetallic tube via friction stir extrusion of aluminium chips

Riccardo Puleo[1] · **Muhammad Adnan**[1] · **Giuseppe Ingarao**[1] · **Livan Fratini**[1]

Received: 27 November 2025 / Accepted: 9 April 2026

Abstract
Bimetallic tubes are employed in applications where a single component must satisfy multiple performance requirements, for instance, combining high strength with corrosion resistance. In literature, manufacturing processes like rotary piercing, forward/backward extrusions, and tube cladding have been commonly used to produce high-performance bimetallic tubes, typically starting from bulk materials. Moreover, recently, new sustainable processes belonging to the solid-state recycling (SSR) category, namely friction stir extrusion (FSE), have also been adopted for tube manufacturing. However, both conventional and SSR-based approaches generally rely on multi-step routes involving pre-heating, homogenization, or pre-consolidation to obtain workable billets, which increases energy consumption. This study goes beyond the limitations of existing extrusion-based recycling processes, proposing a single-step FSE approach that directly converts AA7075 and AA2024 aluminum chips into bimetallic tubes, offering a sustainable upcycling pathway without pre-heating or pre-consolidation stages. Three combinations of rotational speed and axial load were investigated to assess their influence on tube quality. The resulting bimetallic tubes were characterized through microstructural and macrostructural analyses, which revealed the absence of voids and inclusions at the bonding interface, the material composition, a grain refinement (avg. 4.6 μm), and an enhanced hardness (up to 175 HV) under optimal processing conditions. As a matter of fact, this process opens new opportunities for the fabrication of bimetallic tubular components, which can be used in electrical, structural, lightweight, and corrosion-resistant applications.

Keywords Bi-metallic · Friction stir extrusion · FEM · Recycling

1 Introduction

In many industrial sectors, the mechanical and thermal properties of a single material are often insufficient to meet the diverse property requirements of a component. Nowadays, an increasing demand for bimetallic tubes is visible due to the need to address the mechanical properties requirement issues, also aiming to offer enhanced and complementary properties [1]. An example is the automotive sector, where bimetallic tubes are widely employed in exhaust systems to withstand high temperatures while maintaining corrosion resistance and structural rigidity.

One of the most common materials often used across various industries, particularly in aerospace and aeronautics, is aluminium and its alloys. This metal is usually preferred, among others, due to its favorable strength-to-weight ratio. Specifically, the 2xxx and 7xxx series aluminium alloys are notable for their superior mechanical properties and corrosion resistance [2]. In this regard, developing efficient and cost-effective manufacturing techniques for bi-metallic aluminium tubes has become increasingly important to meet industry needs and promote material efficiency.

Currently, various techniques have been explored for the fabrication of bimetallic tubes, including conventional extrusion [3], the hydroforming technique [4], and magnetic pulse cladding [5], etc. These methods primarily rely on

✉ Muhammad Adnan
muhammad.adnan06@unipa.it

Riccardo Puleo
riccardo.puleo01@unipa.it

Giuseppe Ingarao
giuseppe.ingarao@unipa.it

Livan Fratini
livan.fratini@unipa.it

[1] Department of Engineering, University of Palermo, Viale delle Scienze, Palermo 90128, Italy

Published online: 21 April 2026

mechanical bonding, where interfacial adhesion is achieved through plastic deformation induced by applied pressure. However, such bonds often exhibit low strength and are prone to failure at elevated temperatures. To address these limitations and promote atomic-level bonding, advanced techniques such as spin bonding [6] and shear-assisted extrusion with localized heating have been investigated. Although spin bonding can achieve strong metallurgical interface bonding, the experimental setup is highly complex, resulting in increased manufacturing costs. Explosive cladding has also been employed to fabricate bimetallic tubes [7, 8], demonstrating excellent metallurgical bonding at the interface. Nonetheless, this method often leads to undesirable effects such as non-uniform outer diameters, high surface roughness, and significant safety concerns due to the use of explosives. Therefore, there is a clear need to develop a cost-effective, safe, and simplified manufacturing process capable of producing high-quality bimetallic tubes with reliable interfacial strength. Additionally, Ce Ji et al. [9] developed composite tubes using 45-grade carbon steel and 316 L stainless steel via a three-roll skew rolling process. Yuling Chang et al. [10] fabricated thin-walled Cu/Al composite tubes through a spinning process that effectively converted plate materials into tubular forms. Bao Wang et al. [11] successfully produced Ni/Al composite tubes by layering Ni and Al foils, followed by gas expansion and forming. Wei Zhang et al. [12] introduced Mg/Al composite tubes using a modified hot extrusion method, which involved adjusting the die geometry to enhance shear forces and achieve a flat bonding interface. However, the extrusion ratio was limited to around 7 due to constraints associated with the billet and die design.

Recently, driven by the increasing demand for more sustainable manufacturing approaches, environmentally friendly processing techniques have attracted growing interest within the research community. Solid-state recycling (SSR) processes, in particular, have gained significant attention as they aim to reduce the environmental impact of conventional manufacturing routes by enabling the direct recycling of metallic materials. In this context, friction stir-based processing of metal scraps has been widely investigated as a valid approach. The effectiveness of friction stir processing applied to aluminum machining waste was reviewed by Adi et al. [13], who addressed the sustainability challenges of aluminum recycling within a circular economy framework, with particular emphasis on chip consolidation mechanisms and on the factors influencing the final density and microstructure of the recycled material.

Among the friction stir-based processes, FSE has emerged as an innovative technology in metal recycling, offering a sustainable and energy-efficient method for converting scrap or waste metal into valuable components [14, 15]. While FSE is widely recognized for its application in wire production, its potential for manufacturing tubes is increasingly being explored. Literature indicates that most existing tube fabrication methods require multiple processing steps, typically involving at least one high-temperature operation; nevertheless, extrusion remains the most frequently used technique [16]. In contrast, the FSE process offers a more energy-efficient alternative, requiring fewer steps and lower processing temperatures [17]. Despite its advantages, no prior research has been reported on the fabrication of bimetallic tubes combining aluminium 7xxx and 2xxx series alloys using the FSE method. Moreover, the friction stir extrusion of tubes has been commonly performed starting from a bulk component [18–20] or a pre-consolidation step that primarily turns recycling chips into a billet [16], which increases the energy demand of the process. Therefore, a more sustainable approach that aims to reduce the impact on chips recycling and the steps needed for tube production is still missing.

For this reason, this study aims to demonstrate the capability of FSE for directly turning AA2024 and AA7075 recycling chips into high-quality aluminium bimetallic tubes by skipping any preliminary pre-consolidation or pre-heating step. Specifically, the FSE technique has been adopted to fabricate bimetallic tubes consisting of AA7075 as the outer tube and AA2024 as the inner tube. The process is structured in two stages: outer tube production (AA7075) and inner tube production (AA2024).

The experimental campaign was performed at 15 kN vertical load and three different rotational speeds equal to 500, 750, and 1000 rpm. The microstructural evolution at the bonding interface, along with the mechanical properties of the extruded bimetallic tubes, was comprehensively characterized using optical microscopy (OM), scanning electron microscopy (SEM), and microhardness testing. The results confirmed the feasibility and effectiveness of the FSE process in producing multilayered aluminium components with refined microstructures and robust interfacial bonding.

2 Experimental procedures

For the outer tube, AA7075 aluminium alloy chips were used, whereas AA2024 aluminium alloy chips were considered for the inner one because of the different material ductility. Table 1 shows the chemical compositions of the Starting material, i.e., AA7075-T6 and AA2024-T3 aluminium alloy, used in this work. The recycling chips were produced from the milling operation of AA7075-T6 round bar and the turning operation of AA2024-T3 bar. Additionally, the chips were submerged in the acetone for effective cleaning before processing.

Table 1 Chemical composition analysis of AA2024-T3 [21] and AA7075-T6 [22] aluminum alloys

Material	Al	Cu	Mn	Mg	Si	Fe	Cr	Zn
2024-T3	Bal.	4.91	0.54	1.31	0.145	0.31	0.09	0.10
7075-T6	Bal.	1.5	0.3	2.6	0.4	0.5	0.22	5.4

2.1 Experimental campaign

The experimental tests were performed on an ESAB LEGIO Friction Stir Welding machine, specifically adapted for producing aluminium tubes from recycled chips. The FSE process was structured in four different steps: AA7075 chips loading, AA7075 tube extrusion, AA2024 chips loading, and AA2024 tube extrusion. A schematic diagram of the FSE-based bimetallic tube extrusion process is presented in Fig. 1.

In the first step, 20 g of AA7075 aluminium alloy chips were placed into a custom-designed split die (Fig. 2a), which had an internal diameter of 25 mm and a height of 76 mm. The die was manufactured and securely assembled to a backing plate using bolts and nuts. The chips were compacted using a 25 mm diameter flat-head H13 steel tool (Fig. 2b) under an axial force of 5 kN. This compaction is part of the chips' preparation and aims to ensure uniform density, die filling, and to avoid scattering during extrusion. The outer tube was then extruded using a 23 mm diameter tool with a 20° conical taper profile (Fig. 2c). It is worth mentioning that the conical profile was used instead of a flat one to promote smooth material flow and easy tool insertion [20]. After the outer tube was extruded, 20 g of AA2024 aluminium alloy chips were poured into the internal cavity of the previously extruded tube. These chips were compacted using a flat tool of 23 mm diameter, again under a force of 5 kN. The inner tube was then extruded using a 21 mm diameter tool with the same 20° conical taper profile. The tests were performed at 15 kN vertical load and three rotational speeds equal to 500 (low), 750 (medium), and 1000 (high) rpm. The selected ranges of rotational speed and vertical force were defined based on a preliminary experimental campaign aimed at identifying suitable process parameters while ensuring compliance with the machine load capacity, particularly with respect to the maximum allowable vertical force. Moreover, the selected rotational speeds provide a suitable window for investigating the tube bonding

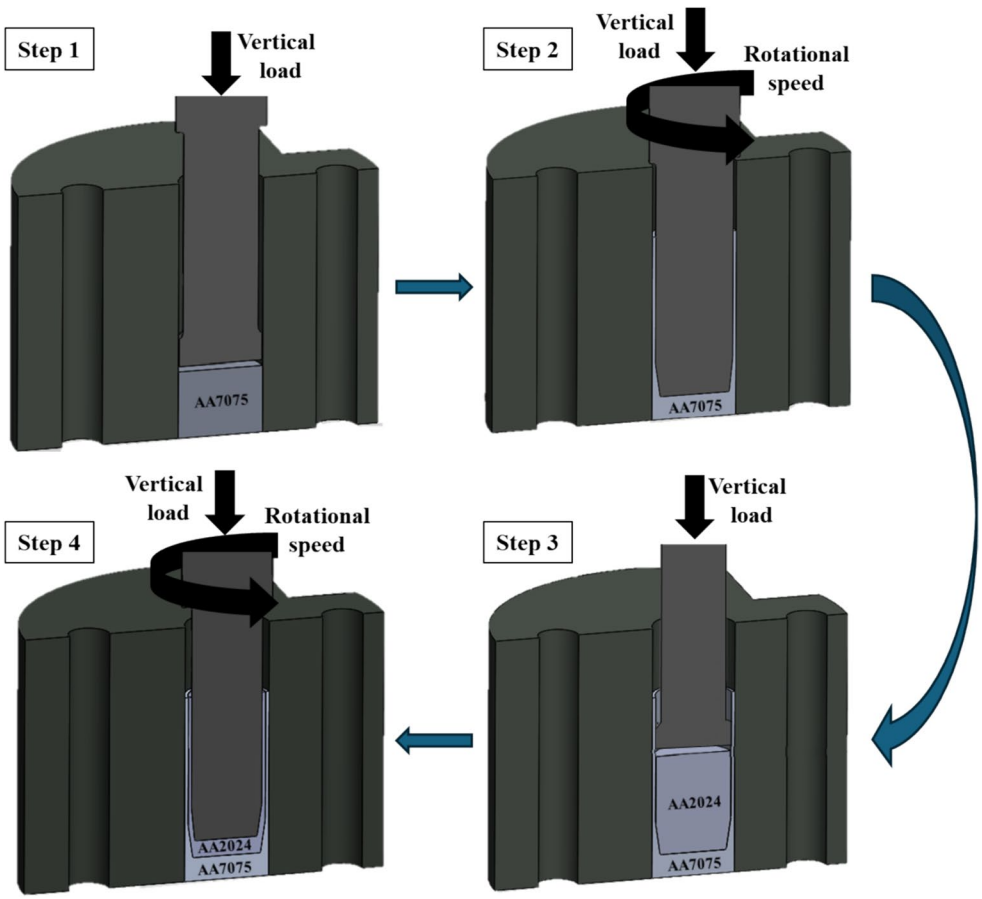

Fig. 1 Schematic diagram of FSE bimetallic tube extrusion process: AA7075 chips compaction (Step 1), AA7075 tube extrusion (Step 2), AA2024 chips loading and compaction (Step 3) and AA2024 tube extrusion (Step 4)

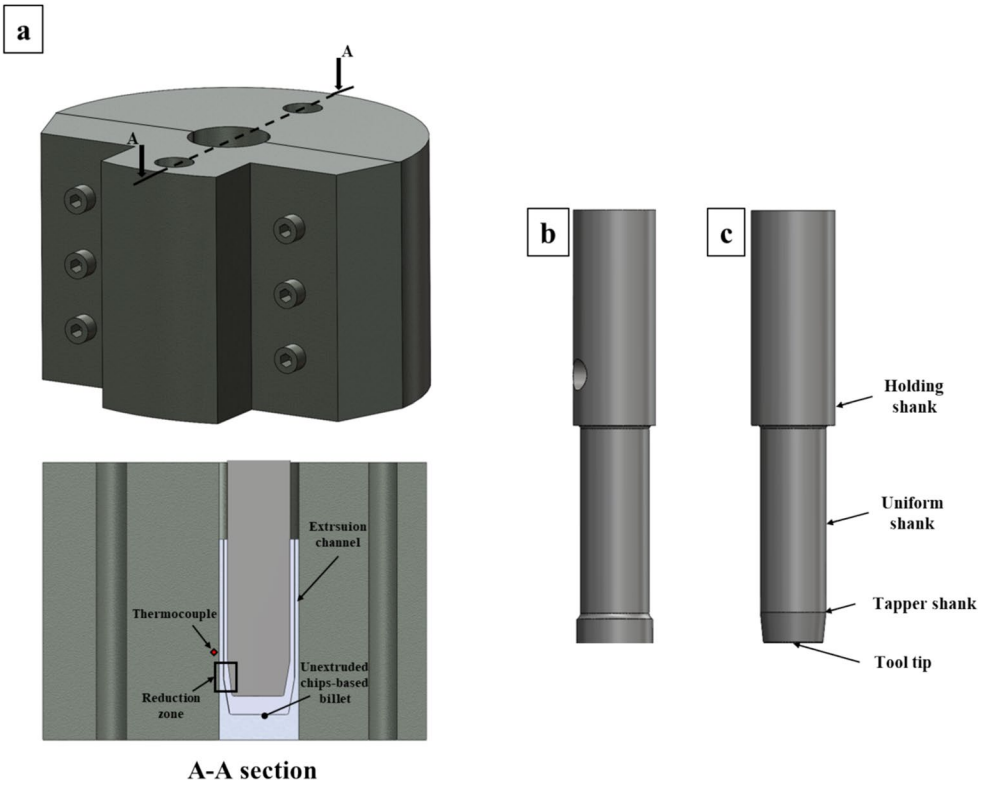

Fig. 2 Sketches of the (**a**) designed die with section, (**b**) compacting tool, and (**c**) 20° tapered tool

behavior, avoiding insufficient chip consolidation at lower rotational speeds and hot cracking phenomena at higher rotational speeds.

In the current study, the outer layer of the bimetallic tube (AA7075) had an average thickness of approximately 1.0 mm, as well as the inner layer (AA2024). Details of the tool geometries are shown in Table 2, while process parameters, including rotational speed and axial extrusion force, are summarized in Table 3.

It is worth mentioning that for monitoring temperature during the extrusion process and for tuning the numerical simulations, a K-type thermocouple was inserted into a hole drilled at 1/3-height of the die, positioned 1 mm from the inner die wall (Fig. 2a, A-A section).

Consequently, the bimetallic tubes were cut longitudinally to the extrusion direction to prepare samples for mechanical and microstructural evaluation. The cross-sections were mounted, ground, and polished, then etched with Keller's reagent (consisting of 2 mL HF, 3 mL HCl, 5 mL HNO_3, and 190 mL H_2O) to expose their microstructural details. Optical microscopy (OM), along with SEM and EDS, was utilized to study the internal structure and elemental distribution, particularly at the bonding interface. The grain size was quantified using the mean linear intercept technique. For mechanical assessment, Vickers microhardness tests were conducted using a 0.5 kg load and a 15-second dwell time. Hardness measurements were taken across the wall thickness of the tube, starting from the outer diameter toward the inner surface, at intervals of approximately 0.2 mm. Each point was tested three times, and the average of the results was used to ensure consistency and reliability. The flattening test was performed through radial-axis compression using the tensile testing machine Galdabini Quasar 600, at a traverse speed of 2.5 mm/min. This method, aligned with ISO 8492 guidelines, enables the assessment of radial deformation capacity and stress-strain behavior under controlled loading.

2.2 Numerical campaign

A numerical campaign was performed using the commercial finite element software SFTC DEFORM 3D. The numerical setup involves five components: a die, a backing plate, two tools, and material chips (Fig. 3). The modelling of the chips batch is complex, and for this reason, the aluminium chips were considered as a single block porous material,

Table 2 Geometry characterization of tapered tools

Tool	Material	Uniform shank (Ø)	Tool tip	Holding shank	Tapered length	Uniform shank
For AA7075	H-13 tool steel	23 mm	22 mm	Ø 30 mm	10 mm	70 mm
For AA2024	H-13 tool steel	21 mm	20 mm	Ø 30 mm	10 mm	70 mm

Table 3 FSE process parameters and tube material layers disposition

ID	Rotational speed [rpm]	Force [kN]	Total tube thickness [mm]	Outer tube	Inner tube
ID1	500	15	2	7075	2024
ID2	750	15	2	7075	2024
ID3	1000	15	2	7075	2024

following the material formulation of Shima-Oyane [23]. Specifically, an initial relative density value of 0.7 was assigned to the porous billet, calculated experimentally considering the mass of the loaded chips and the geometry of the die's chamber. The porous billet was characterized by a mesh size of 35,000 elements with a refining mesh window close to the tool-material contact (Fig. 3, A-A section).

The other components were considered as rigid material made of H-13 steel. The two tools were defined by a mesh size of 60,000 elements, while for both the die and backing plate, the mesh size was 30,000 elements. A tuning approach was performed for calculating the proper thermal and frictional coefficients. In this regard, the experimental data of the thermocouple were tuned to the numerical one, and the following values were obtained: shear factor of 0.2 and interface heat transfer coefficients (IHTC) of 11, 45, and 45 W/mm²/K for the tool-material, die-material, and backing plate-material contacts, respectively. The methodology of this numerical calibration has already been applied and assessed in the literature [24].

3 Results and discussion

3.1 Macroscopical analysis

Figure 4 depicts the bimetallic tubes fabricated from AA7075 and AA2024 aluminum alloy chips using the FSE process under various process parameters. All tubes were successfully extruded, demonstrating the viability of the FSE technique. However, surface quality and material consolidation varied with processing conditions.

At the beginning of the process, the material is compressed and heated up thanks to the initial stirring and frictional actions of the tool. In these early stages, proper process parameters are crucial for obtaining optimal chips bonding and high surface quality. In this regard, when the

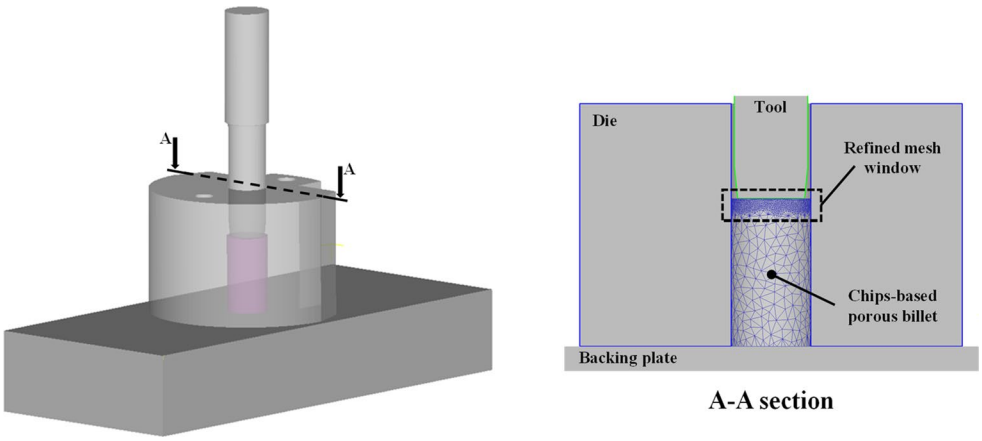

Fig. 3 Numerical setup for the FSE bimetallic process and section of the parts

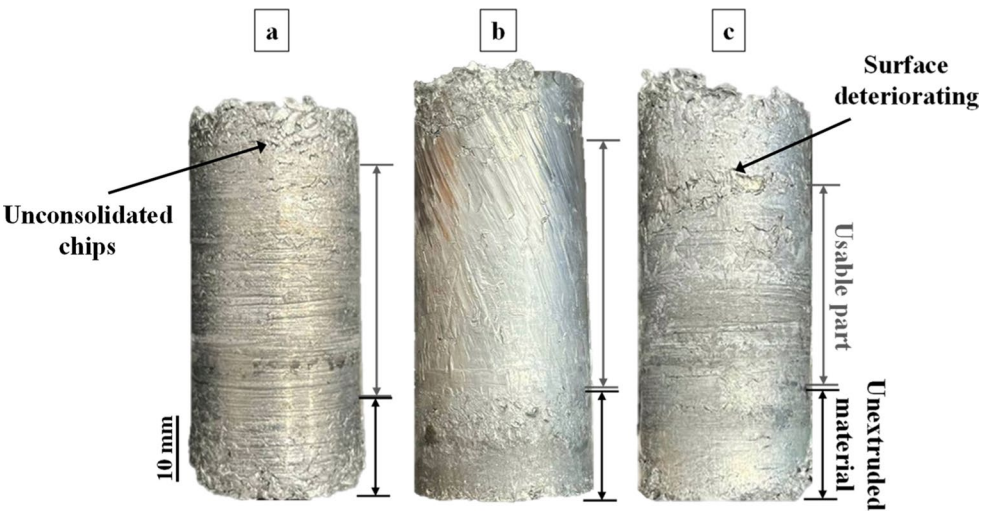

Fig. 4 Macroscopical observations of bimetallic tubes through the FSE process for (**a**) ID1, (**b**) ID2, and (**c**) ID3

heat generated is too low (ID1, Fig. 4a), a lack of consolidation of the first extruded layers is visible near the top surface of the tube. On the other hand, at a high rotational speed (ID3, Fig. 4c), excessive heat led to early softening of the material, which resulted in the surface deteriorating and uneven surface roughness in large parts of the extruded tube. At a medium rotational speed (ID2, Fig. 4b), optimal surface conditions were achieved. At process parameters ID2, the tube exhibited a uniform and quite smooth outer surface with no visible cracks at the top. Additionally, the bottom surface showed no signs of adhesion between the backing plate and the workpiece material, indicating effective material flow. It is worth remarking that the material behavior of AA7075 recycling chips plays an important role in material bonding; high mechanical properties may hinder proper consolidation. Difficulty in chips bonding for AA7075 recycling chips was also experienced by Puleo et al. [24] in the friction stir consolidation process.

The final length of the bimetallic tube, after trimming both top unconsolidated chips and bottom consolidated billet, was approximately 40 mm.

The resulting average thickness of the produced tubes, along the radial direction, is represented in Fig. 5. For ID1 and ID3 (Fig. 5), a non-uniform thickness distribution was observed. In the case of ID1, characterized by a low rotational speed and limited heat generation, the material exhibits insufficient softening. Under these conditions, the small tool eccentricity caused by manual positioning inside the chamber was amplified, leading to unstable material flow during extrusion. The reduced plasticity increased flow resistance and process vibrations, resulting in significant thickness variability between the inner and outer tubes. On the other hand, ID2 exhibited the most stable extrusion conditions, as also suggested by the smoother surface finish. This demonstrates a balanced thermo-mechanical state that promoted a more controlled material flow, leading to improved thickness uniformity with a limited deviation

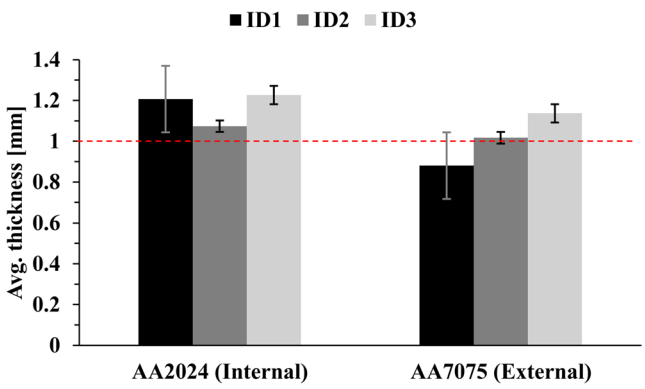

Fig. 5 Average thickness measurement for both internal and external tubes at process windows: ID1, ID2, and ID3. In red, the nominal diameter of each tube

(approximately 0.07 mm). For ID3, the higher rotational speed produced excessive heat input, leading to pronounced material softening. In these conditions, the reduced effective extrusion pressure (softening) combined with the deterioration of the surface results in an overall increase and variability of the tube thickness. Despite the observed thickness variations, more or less pronounced depending on the case study, the tubes did not exhibit any evident ovality.

Concerning the external surface roughness, from a qualitative point of view, the resulting surface morphology reflects the chip-based nature of the manufacturing process. Indeed, when comparing tubes produced from bulk material [18–20] with those obtained from chips [16], noticeable differences in the external surface can be observed.

3.2 Microstructural investigations

Figure 6 illustrates the cross-sectional microstructure of the AA7075/AA2024 bimetallic tube fabricated under different process parameters. In Fig. 6a, corresponding to the low rotational speed condition (ID1), insufficient bonding is observed at the interface between the two materials. A distinct interfacial separation indicates that the heat generated during the process was insufficient to promote effective metal-to-metal bonding. High-magnification imaging of the interface further reveals the presence of unbonded regions. In contrast, Fig. 6b and c, corresponding to the medium (ID2) and high (ID3) rotational speed conditions, show less visible surface defects in the cross-section. Especially for ID3, the interface appears continuous and free from voids or delamination, indicating successful consolidation and the formation of a structurally sound bimetallic tube.

At higher magnification (third column of Fig. 6), the interfacial bonding between the two alloys is attributed to a diffusion-assisted mechanism promoted by severe plastic deformation and elevated temperatures generated during the FSE process (yellow dashed lines in Fig. 6c). Although a quantitative characterization of the interfacial diffusion layer was not performed in the present work, the observed interfacial morphology is consistent with diffusion-controlled bonding reported for similar FSE-based bimetallic tube fabrication processes. In particular, Swarnkar et al. [19] demonstrated the formation of micrometrical interdiffusion layers and intermetallic compounds through EDS and XRD analyses under comparable processing conditions. The gradual change in contrast observed within this region in the EDS maps further supports the occurrence of interdiffusion phenomena, contributing to effective solid-state bonding without the formation of interfacial defects.

For investigating the microstructure of the bimetallic tubes at the interface, SEM analysis was performed. Figure 7 presents SEM micrographs along with corresponding EDS

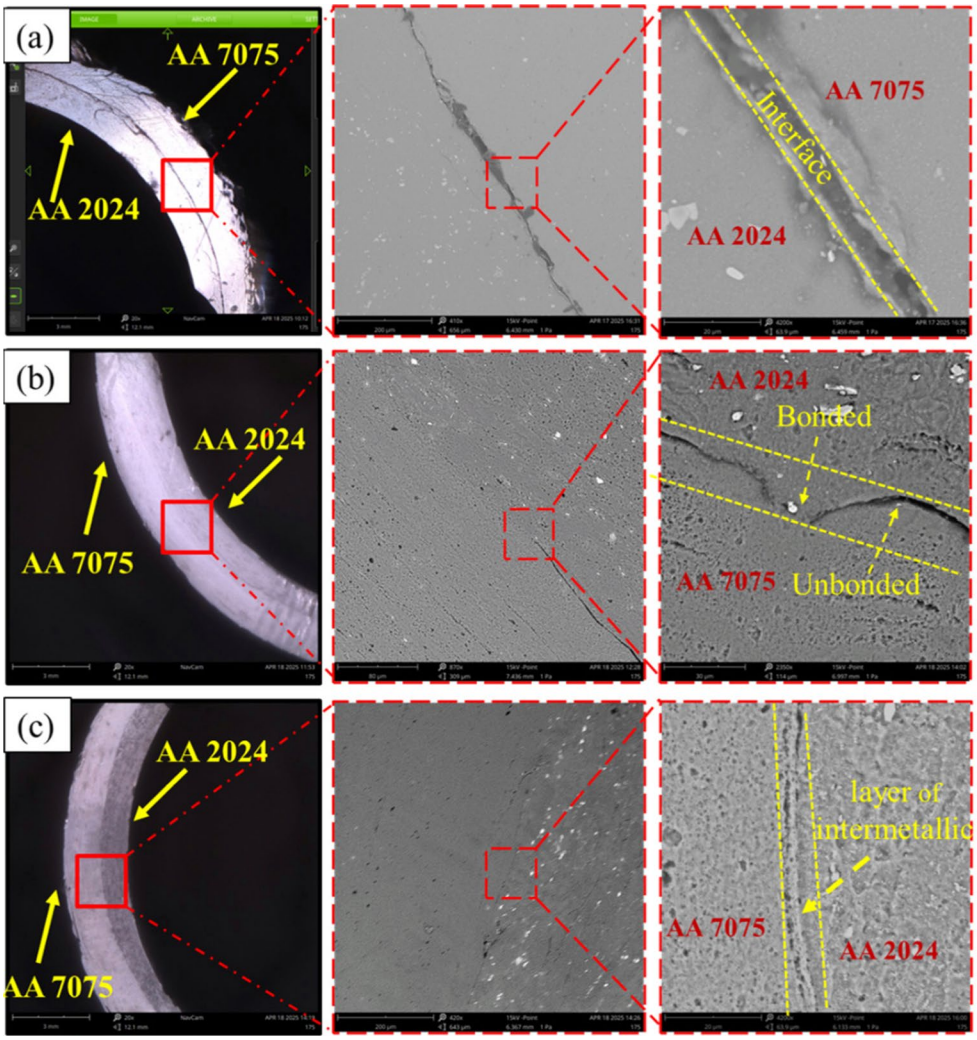

Fig. 6 Microstructure of the cross-section of the bonding layer in AA7075/2024 bimetallic tube prepared by different process methods (**a**) ID1, (**b**) ID2, and (**c**) ID3

results, focusing on the transition zone between AA2024 and AA7075, marked by a red dashed line. Figure 7a (ID1), at low rotational speed, displays discontinuity and areas of insufficient bonding, indicating that the heat generated during the process was not adequate to achieve full metallurgical joining. It is important to note that, to enhance the visualization of the lack of bonding, the image was acquired at a higher magnification than those reported for ID2 and ID3 (Fig. 7b and c, respectively). In contrast, the samples extruded at medium and high rotational speeds (ID2 and ID3) haven't shown any signs of discontinuity in the transition region. Additionally, the EDS mapping presented in Fig. 7 further validates and supports the quality of the bond. In this regard, the images of ID1 clearly delineate the transition zone between the AA7075 and AA2024 alloys, with an elemental distribution that matches the expected chemical composition of each material. Specifically, zinc (Zn) was predominantly detected in the AA7075 region, while copper (Cu) was more concentrated in the AA2024 region. On the contrary, ID2 and ID3 show more elemental diffusion. This elemental distribution provides strong evidence of alloying elements' diffusion across the interface and metallurgical bonding between the two aluminium alloys, processed via the FSE process.

Further grain size analysis was performed on the cross-section of the bimetallic tube to enhance microstructural characterization. Quantitative measurements of the grain dimension are reported in Fig. 8. Relatively fine grains were observed near the outer surface of the AA7075 tube, with average values of approximately 4.64 µm for ID1, 4.30 µm for ID2, and 4.11 µm for ID3. Moving toward the interface, the grain size slightly increases, attaining average values of 5.65 µm, 4.99 µm, and 4.45 µm, respectively. Finally, near the inner surface of the AA2024 tube, a fine and equiaxed grain structure is again observed, with average grain sizes of 4.60 µm for ID1, 4.53 µm for ID2, and 4.63 µm for ID3.

A similar trend has already been reported during friction stir back extrusion of AA6063 and magnesium tubes by Zhang et al. [25] and Jarrah et al. [26], respectively. In both studies, an increase in grain size from the inner to the

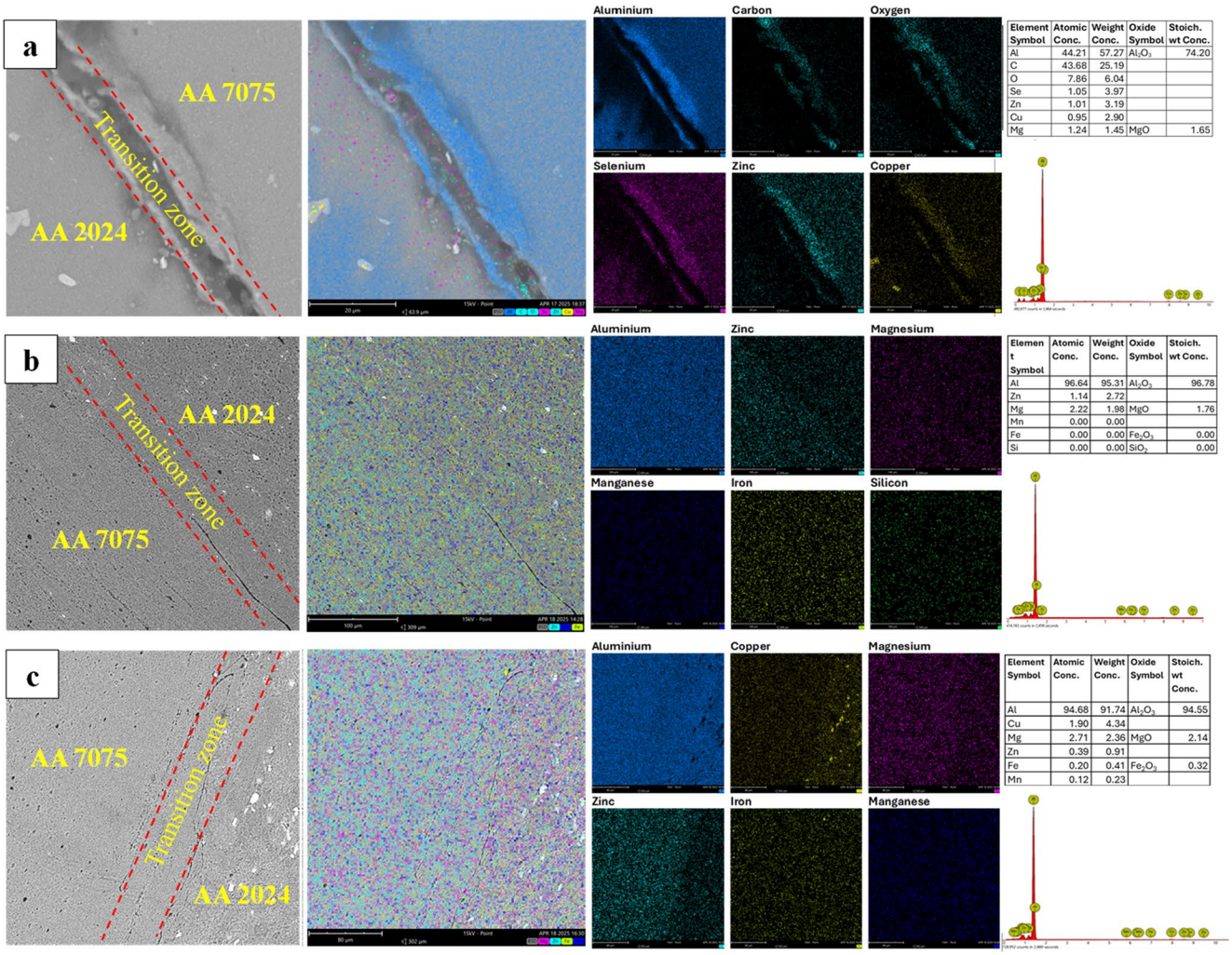

Fig. 7 SEM microstructure of the transition zone of the bimetallic tube, along with EDS mapping for (**a**) ID1, (**b**) ID2, and (**c**) ID3

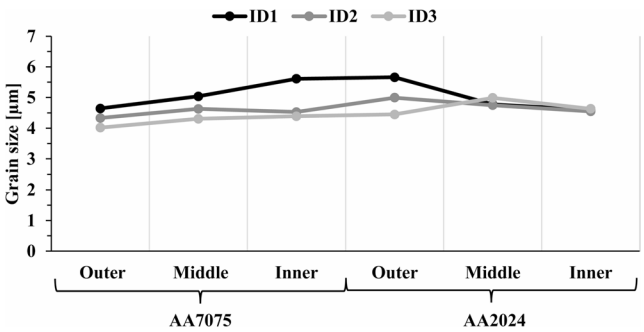

Fig. 8 Average grain size of the bimetallic tube evaluated from the outer to the inner surface, for each ID

outer surface of the produced tube was observed. A comparable phenomenon was also investigated by Baffari et al. [27] during wire production via the FSE process. As stated by the authors, the material in direct contact with the tool, which is forced through the extrusion reduction zone, is subjected to high pressure and temperature, which promote dynamic recrystallization and grain refinement. Looking at the ID1 case study, these trends are evident for the AA2024 tube (Fig. 8). The severe plastic deformation experienced at the inner surface enhances recrystallization phenomena, leading to a visible grain size reduction. However, this trend is not visible for the AA7075 tube; the production of the second tube (AA2024) thermally affected the microstructure of the first one (AA7075), resulting in grain growth, particularly at the interface. On the contrary, in the case studies ID2 and ID3, due to the limited thickness, the improved processing conditions (higher rpm and stirring) led to a more uniform thermo-mechanical history, which promoted a more consistent recrystallization across the section and, consequently, a more homogeneous grain size distribution. Further details on the role of the temperature and strain are discussed in Sect. 3.3.

Microstructural images along the radial direction of the tube are presented in Fig. 9, acquired from three representative regions: the outer surface of the AA7075 tube, the AA7075/AA2024 interface, and the inner surface of the AA2024 tube. The grain size at the inner and outer surfaces (first and third columns) appears comparable across all IDs. On the other hand, at the interface, the grain size in ID1 (Fig. 9a) is visibly larger than in ID2 and ID3 (Fig. 9b, c). No appreciable differences are observed between ID2 and ID3, consistent with the observations in Fig. 8.

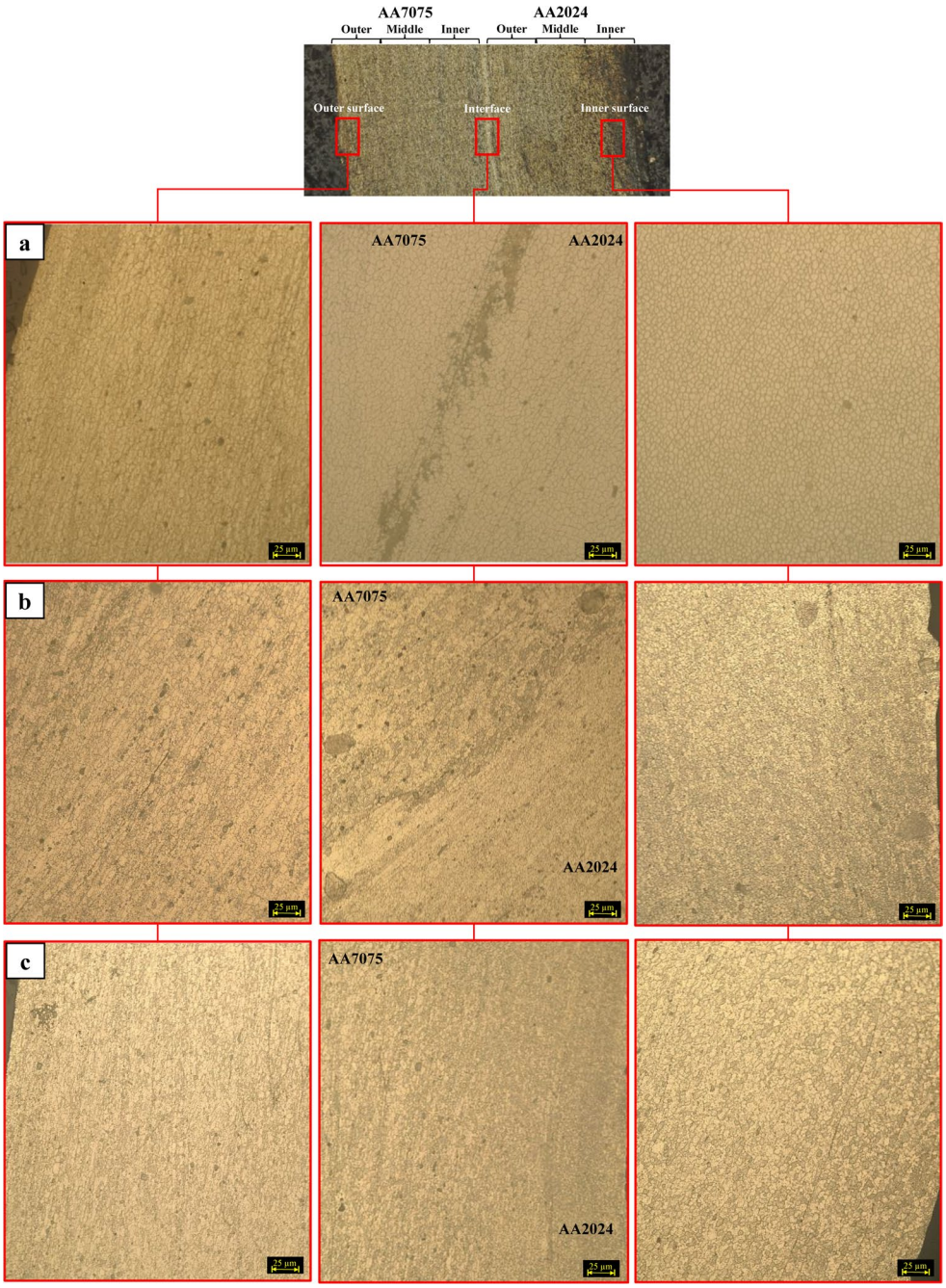

Fig. 9 Microstructure of the bimetallic tube in the outer surface of the AA7075 tube, AA7075/AA2024 tube interface, and the inner surface of the AA2024 tube, for (**a**) ID1, (**b**) ID2, and (**c**) ID3. Columns represent the observation zone, while the rows represent the IDs

3.3 Numerical results and microstructural comparison

To support the experimental findings, numerical simulations were conducted to provide an overview of the temperature and strain behavior during FSE tube processing (Fig. 10). In this regard, a plot of the temperature and strain profiles at the same process time for AA7075 tube production has been proposed for case study ID1 (Fig. 10a) and ID3 (Fig. 10b). The results reveal that high strain levels occurred both across

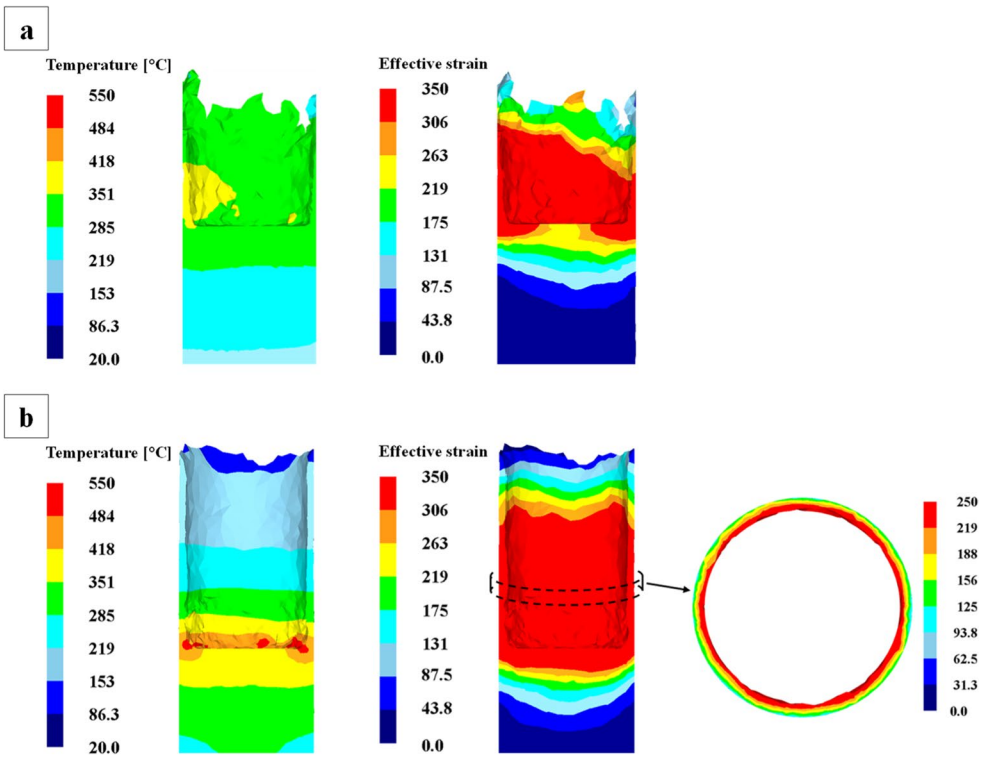

Fig. 10 Temperature and effective strain results for (**a**) ID1 and (**b**) ID3 (with a zoomed view of the cross-section)

the tube thickness and under the tool. Moreover, the detailed cross-sectional view in Fig. 10b indicates that the strain is not uniformly distributed through the tube's thickness; instead, it visibly increases from the outer surface toward the inner one. This strain distribution demonstrates that the tool stirring action is more emphasized at the inner tube's surfaces than the external one, corroborating the observation regarding the occurrence of recrystallization phenomena in the inner surface, previously discussed. Regarding temperature profiles, the comparison between ID1 and ID3 revealed that ID1 exhibited a lower temperature range (280–350 °C), uniformly distributed along the tube. This condition, combined with longer processing times required to achieve the final tube length, is responsible for the slight increase in grain size observed for ID1 in Fig. 8. Conversely, ID3 is characterized by a more localized temperature-affected zone (ranging between 300 and 500 °C). As a matter of fact, the improved material softening due to the combination of high localized temperature and intense strain, induced by material stirring, eases the tube production and promotes faster thermal dissipation.

Finally, the length and surface quality of the ID3 tube clearly demonstrate the process's stability under appropriate processing conditions, thereby supporting the previous considerations.

Numerical simulations were also employed to further investigate and explain the grain growth phenomena observed at the interface of the bi-metallic tube (Fig. 8). A point-tracking approach was adopted to track the temperature evolution of a selected point over the entire process. In particular, a point, initially located at the interface of the AA7075 extruded tube, was tracked from the considered process time backward to the beginning of the process (Fig. 11).

The point-tracking results showed that, during the FSE process, the material in contact with the tool, particularly near the extrusion channel, reached the highest temperatures, ranging from 480 to 550 °C (Fig. 12). During the AA7075 extrusion stage (Fig. 12a), the tracked point moved from the initial position (under the tool) toward the tube wall, experiencing a peak temperature of approximately 400 °C, which lies within the recrystallization temperature range for aluminium alloys. Under these conditions, the combined effect of high strain and elevated temperature promoted recrystallization, resulting in grain refinement of the AA7075 alloy. During the production of the AA2024 tube, point-tracking analysis revealed that the temperature at the monitored location increased again to approximately 350 °C (Fig. 12b), partly due to thermal exchange with the already processed AA7075 tube. This secondary temperature peak, located within the recrystallization range, acted as an additional thermal cycle, leading to grain coarsening at the interface in both materials. For this reason, the grain size in correspondence to the AA7075 inner zone resulted in being bigger than the outer (Fig. 9), despite the fact that the tool refined the inner portion of the AA7075 tube.

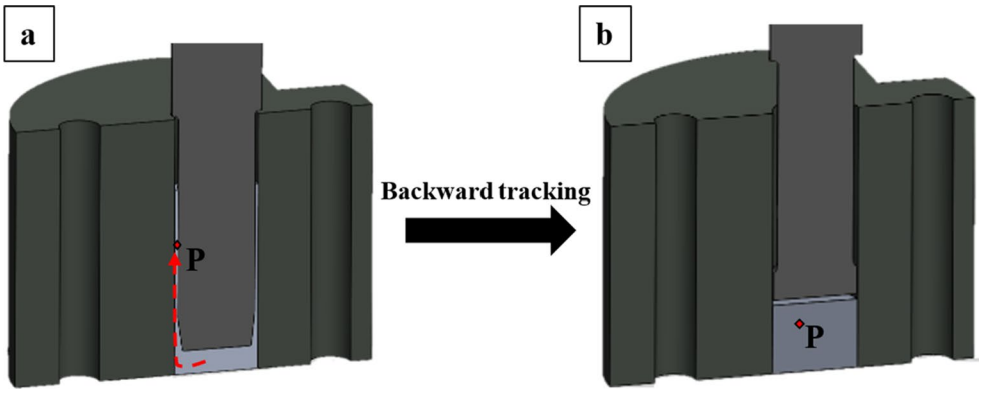

Fig. 11 Point tracking approach from the (**a**) final position (tube extrusion), backward to the (**b**) initial position

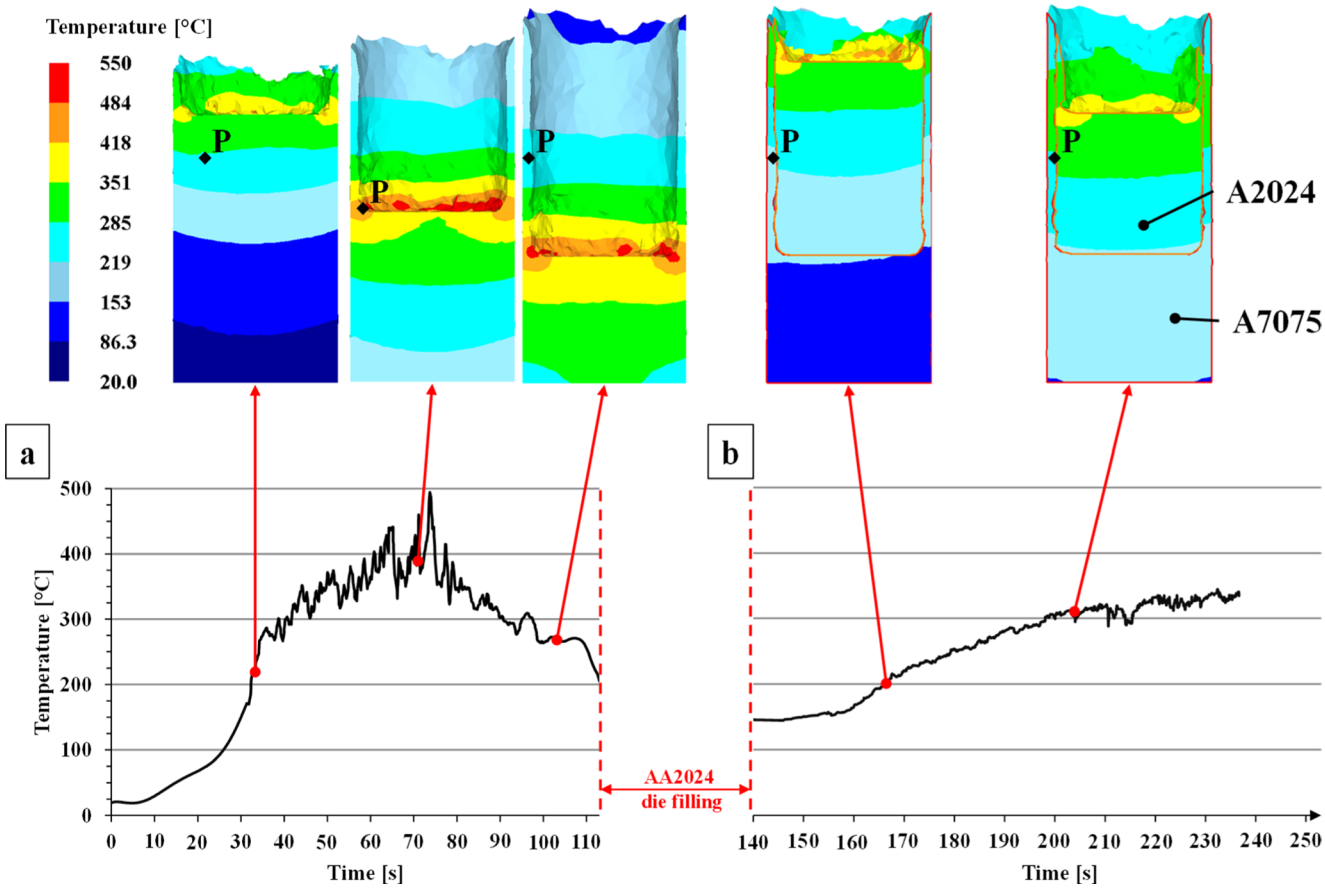

Fig. 12 Numerical simulation results: (**a**) recording point location for temperature acquisition, (**b**) strain distribution of the cross section of the numerical AA7075 tube, and (**c**) temperature evolution of the extruded tubes, for ID3

3.4 Hardness and mechanical characterization

The mechanical properties of the obtained bimetallic tube were investigated through Vickers microhardness measurements by performing twelve indentation points (Fig. 13b) along the cross-section of the tube and flattening tests. The results of these measurements are reported in Figs. 13a and 14.

Typically, regions containing unbonded or poorly bonded chips exhibit lower hardness compared to areas where strong metallurgical bonding has occurred. Data shows noticeable variation in hardness along different paths across the thickness of the tube. Compared to the average Vickers hardness of the base material, all measured values were higher, indicating that the FSE process enhances the mechanical properties of the extruded material. A consistent trend was

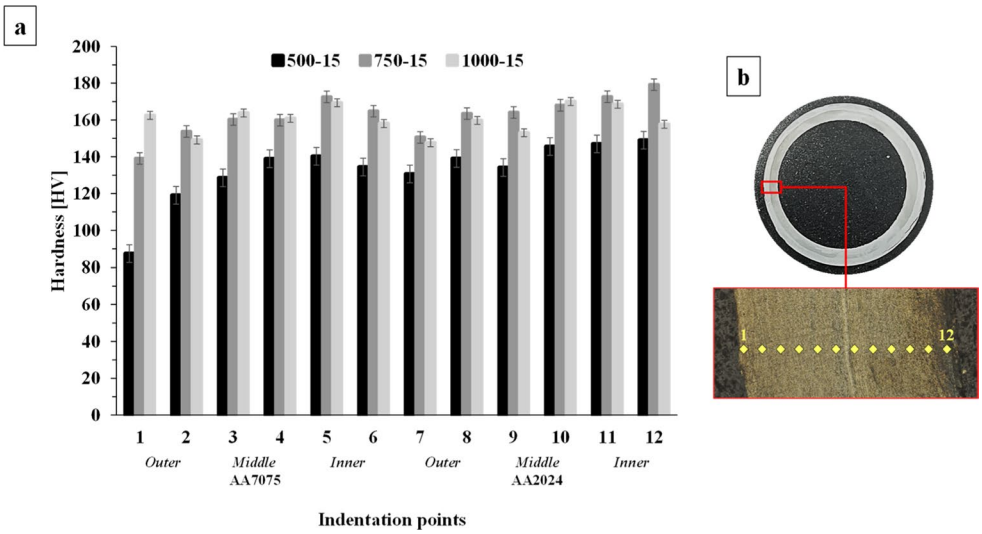

Fig. 13 (**a**) Average hardness of bimetallic tube for ID1, ID2, and ID3, and (**b**) indentation points considered for the hardness measurement

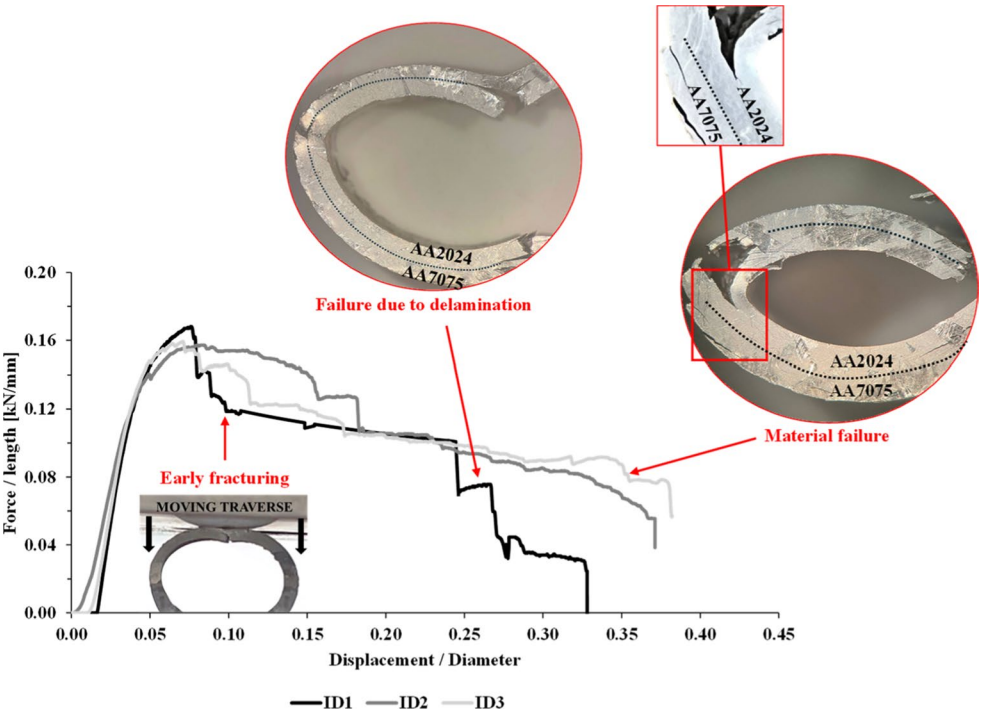

Fig. 14 Flattening test results for ID1, ID2, and ID3, normalized to the tube length and external diameter

observed for ID1: microhardness values increased progressively from the outer surface toward the inner surface. For instance, the hardness at point 1 (outer surface) was 87 HV, which increased to 149 HV at point 12 (inner surface). A more constant trend was instead noted for other process conditions. This improvement aligns with the observations made by Baffari et al. [27]. In his work, the authors found that after the FSE process, the hardness of the product was close to the T3 heat treatment hardness value. The AA7075 and AA2024-T3 hardness values are typically about 150 and 145 HV, respectively. A similar constant hardness trend was also observed by Zhang et al. [25] during AA6063 tube production via FSE, and Shunmugasamy et al. [28] for the friction stir extrusion of a magnesium tube.

Additionally, an overall increase in hardness has been reported with the increase in rotational speed; at the same vertical load, the increase in rotational speed results in an increase in frictional heating, which enhances chip consolidation, reduces internal voids, and promotes grain refinement, as already shown in Chap. 3.2.

These observations are consistent with the microstructural analysis, which demonstrated grain size refinement from the AA7075 toward the AA2024 layers of the bimetallic tube. However, in the transition zone between AA7075

and AA2024, a localized decrease in microhardness was noted. This reduction resulted from variation in grain size and minor defects such as porosity or unbonded regions, which act as stress concentrators, reducing the overall hardness. Similarly, the external surface of the AA7075 tube exhibited low hardness values due to the roughness and poor quality of the surface [27], especially for ID1.

This microhardness trend is consistent with the flattening test results. Figure 14 reports the force per unit length as a function of the "normalized displacement". In order to enable a meaningful comparison among specimens, the applied force was divided by the specimen length, thus removing the direct geometric dependence on sample height. Additionally, the displacement was "normalized" by the initial external diameter (constant for all specimens), allowing the deformation to be expressed as a percentage of the tube diameter and ensuring comparison at equivalent flattening levels.

Consistent with the microstructural and microhardness observations, ID1 exhibits lower resistance to flattening. This behavior can be attributed to insufficient interfacial bonding and reduced hardness. In fact, early-stage fracture is observed at low displacements (displacement/diameter$\approx$0.1) and is associated with delamination phenomena. After a certain deformation (displacement/diameter$\approx$0.25), delamination propagated to multiple locations, ultimately leading to tube failure.

On the other hand, the comparison between ID2 and ID3 revealed, instead, only minor differences in microstructure and hardness; however, more pronounced variations were observed in terms of external roughness, hot cracking, and thickness uniformity, as reported previously. These features are evident in Fig. 14, particularly in the force-displacement response. Although ID2 exhibits a higher initial load, ID3's improved interfacial bonding yields a more stable response in the later stages of deformation, allowing higher displacement and force levels before final collapse. It is worth noting that, for both ID2 and ID3, failure did not occur as a result of delamination, but rather due to intra-material damage (in the case of ID3, within the AA2024 layer). This resulted in a smoother force–displacement curve, indicative of effective interfacial bonding. Overall, considering the combined microstructural observations, microhardness distribution, and mechanical response under flattening, ID2 represents the most balanced processing condition.

4 Conclusion

In this study, it was proved that FSE can be successfully applied to produce AA7075/AA2024 bimetallic tubes in a single-step process directly from recycled aluminium chips, demonstrating the effectiveness of this upcycling route. Actually, enhanced microstructural and hardness characteristics were observed across the thickness of the tube, along with a detailed SEM analysis of the bonding quality at the tube interface. The key findings are summarized as follows:

- The results demonstrated that the FSE process is a viable method for fabricating bimetallic tubes. Among the evaluated conditions, the tube produced at 750 rpm and 15 kN exhibited superior surface finish, refined microstructure, enhanced microhardness, and thickness uniformity.
- Optical microscopy and grain size analysis revealed uniformly distributed equiaxed grains, and an overall gradual decrease in grain size was observed toward the inner wall, resulting from the tool's thermal and stirring actions. Moreover, microstructural analysis confirmed that adequate process conditions led to dynamic recrystallization, resulting in fine-grained structures (avg. 4.62 µm, at the outer and inner surface of the bi-metallic tube) and effective bonding between dissimilar aluminum alloys, thus contributing to improved microhardness.
- The hardness characterization revealed an overall increase from the outer layer (AA7075) to the inner layer (AA2024). The average hardness for the AA7075 layer was about 150 HV, while a value of nearly 160 HV was obtained for the AA2024 one. At the interface between the two layers, a drop in hardness was observed (around 140 Hv).
- Numerical simulations showed that the material located under the tool and near the extrusion channel experiences high temperatures and strains, conditions that promote recrystallization during FSE. Moreover, a point tracking approach for temperature monitoring at the interface showed that the inner surface of the AA7075 tube is subjected to a secondary heating effect, due to the extrusion of the second tube, which affected the grain size at the tube's interface.
- SEM and EDS analyses verified the presence of a metal-to-metal bonded interface at proper process parameters (750 rpm − 15 kN and 1000 rpm – 15 kN). The thermal and mechanical input during FSE was sufficient to facilitate elemental diffusion across the interface, leading to strong interlayer bonding.
- Flattening tests reinforced and corroborated the microstructural and SEM findings. In particular, these tests revealed that low bonding quality in the 500 rpm – 15 kN condition led to delamination phenomena, whereas sound interfacial bonding in the 750 rpm – 15 kN and 1000 rpm – 15 kN conditions resulted in intra-material damaging.

Further studies will focus on the application of this upcycling route to the manufacturing of tubes made from different aluminium alloys and combinations of dissimilar materials.

Acknowledgements This study was funded by Italian MUR funds through European Union-NEXT Generation EU scheme; title of the project: "Finalizing processes for multi-material based Functionally Graded billets and wires obtained through solid state recycling operations of aluminum alloy chips - FULL RECYCLE", PRIN 2022 (CUP: B53D23006550006).

Author contributions Riccardo Puleo: Numerical campaign development, Draft writing. Muhammad Adnan: Experimental campaign development, Draft writing. Giuseppe Ingarao: Research supervision, Draft, Final revision. Livan Fratini: Research supervision, Paper revision.

Funding Open access funding provided by Università degli Studi di Palermo within the CRUI-CARE Agreement.

Declarations

Competing interest The Authors disclose no actual or potential conflict of interest that could inappropriately influence, or be perceived to influence, this work.

References

1. Swarnkar R, Karmakar S, Pal SK (2023) An investigation of bimetallic tube fabrication through a novel friction stir extrusion based technology for automotive applications. Mater Today Commun 35:106363. https://doi.org/10.1016/j.mtcomm.2023.106363
2. Xie Z, Zhou L, Li J et al (2025) Mechanical and Corrosion Properties of AA2024 Aluminum Alloy with Multimodal Gradient Structures. Met (Basel) 15:177. https://doi.org/10.3390/met15020177
3. Kang CG, Jung YJ, Kwon HC (2002) Finite element simulation of die design for hot extrusion process of Al/Cu clad composite and its experimental investigation. J Mater Process Technol 124:49–56. https://doi.org/10.1016/S0924-0136(02)00106-1
4. Wang X, Li P, Wang R (2005) Study on hydro-forming technology of manufacturing bimetallic CRA-lined pipe. Int J Mach Tools Manuf 45:373–378. https://doi.org/10.1016/j.ijmachtools.2004.09.015
5. Fan Z, Yu H, Li C (2016) Plastic deformation behavior of bimetal tubes during magnetic pulse cladding: FE analysis and experiments. J Mater Process Technol 229:230–243. https://doi.org/10.1016/j.jmatprotec.2015.09.021
6. Mohebbi MS, Akbarzadeh A (2011) Fabrication of copper/aluminum composite tubes by spin-bonding process: experiments and modeling. Int J Adv Manuf Technol 54:1043–1055. https://doi.org/10.1007/s00170-010-3016-5
7. Guo X, Tao J, Wang W et al (2013) Effects of the inner mould material on the aluminium–316L stainless steel explosive clad pipe. Mater Des 49:116–122. https://doi.org/10.1016/j.matdes.2013.02.001
8. Gómez X, Echeberría J (2000) Microstructure and mechanical properties of low alloy steel T11–austenitic stainless steel 347H bimetallic tubes. Mater Sci Technol 16:187–193. https://doi.org/10.1179/026708300101507532
9. Ji C, Niu H, Li Z et al (2024) Deformation law and bonding mechanism of 45 carbon steel/316L stainless steel cladding tubes fabricated by three-roll skew rolling bonding process. J Mater Process Technol 325:118277. https://doi.org/10.1016/j.jmatprotec.2023.118277
10. Chang Y, Chen H, Zhou J et al (2023) Micro-nano interface structure and mechanical characteristics of thin wall Cu/Al composite tubes prepared by strong staggered spinning. Mater Charact 206:113405. https://doi.org/10.1016/j.matchar.2023.113405
11. Wang B, Wang D, Wang S et al (2023) Fabrication of NiAl alloy hollow thin-walled component through hot gas forming of Ni/Al laminated tube and conversion process. J Mater Res Technol 26:7224–7236. https://doi.org/10.1016/j.jmrt.2023.09.057
12. Zhang W, Hu H jun, Hu G et al (2023) A direct extrusion-shear deformation composite process that significantly improved the metallurgical bonding and texture regulation grain refinement and mechanical properties of hot-extruded AZ31/AA6063 composite tubes. Mater Sci Engineering: A 880:145090. https://doi.org/10.1016/j.msea.2023.145090
13. Adi SS, Malik VR (2025) Friction stir processing of aluminum machining waste: carbon nanostructure reinforcements for enhanced composite performance - a comprehensive review. Mater Manuf Processes 40:285–334
14. Adnan M, Buffa G, Baghdadchi A et al (2024) Unveiling the mechanical and microstructural properties of SiC reinforced aluminum wires recycled from scraps by friction stir extrusion. Mater Sci Engineering: A. https://doi.org/10.1016/j.msea.2024.147333. 916:
15. Buffa G, Campanella D, Adnan M et al (2024) Improving the Industrial Efficiency of Recycling Aluminum Alloy Chips Using Friction Stir Extrusion: Thin Wires Production Process. Int J Precision Eng Manuf - Green Technol. https://doi.org/10.1007/s40684-023-00573-w
16. Behnagh RA, Fathi F, Yeganeh M et al (2019) Production of seamless tube from aluminum machining chips via double-step friction stir consolidation. Int J Adv Manuf Technol 104:4769–4777. https://doi.org/10.1007/s00170-019-04326-5
17. Baffari D, Reynolds AP, Masnata A et al (2019) Friction stir extrusion to recycle aluminum alloys scraps: Energy efficiency characterization. J Manuf Process 43:63–69. https://doi.org/10.1016/j.jmapro.2019.03.049
18. Abu-Farha F (2012) A preliminary study on the feasibility of friction stir back extrusion. Scr Mater 66:615–618. https://doi.org/10.1016/j.scriptamat.2012.01.059
19. Swarnkar R, Karmakar S, Pal SK (2023) An investigation of bimetallic tube fabrication through a novel friction stir extrusion based technology for automotive applications. Mater Today Commun 35. https://doi.org/10.1016/j.mtcomm.2023.106363
20. Asadi P, Akbari M, Sadowski T et al (2024) Examining the impact of tool taper angle in Al-Si tube manufacturing by friction stir extrusion. J Manuf Process 131:532–544. https://doi.org/10.1016/j.jmapro.2024.09.047
21. Ahn J, Chen L, He E et al (2017) Effect of filler metal feed rate and composition on microstructure and mechanical properties of fibre laser welded AA 2024-T3. J Manuf Process 25:26–36. https://doi.org/10.1016/j.jmapro.2016.10.006

22. Saravanan V, Banerjee N, Amuthakkannan R, Rajakumar S (2015) Microstructural Evolution and Mechanical Properties of Friction Stir Welded Dissimilar AA2014-T6 and AA7075-T6 Aluminum Alloy Joints. Metallography Microstruct Anal 4:178–187. https://doi.org/10.1007/s13632-015-0199-z
23. Shima SOM (1976) Plasticity theory for porous metals. Int J Mech Sci 18:286–291
24. Puleo R, Latif A, Ingarao G et al (2023) Solid bonding criteria design for aluminum chips recycling through friction stir consolidation. J Mater Process Technol 319. https://doi.org/10.1016/j.jmatprotec.2023.118080
25. Zhang S, Frederick A, Wang Y et al (2019) Microstructure Evolution and Mechanical Property Characterization of 6063 Aluminum Alloy Tubes Processed with Friction Stir Back Extrusion. JOM 71:4436–4444. https://doi.org/10.1007/s11837-019-03852-7
26. Jarrah OM, Nazzal MA, Darras BM (2020) Numerical modeling and experiments of Friction Stir Back Extrusion of seamless tubes. CIRP J Manuf Sci Technol 31:165–177. https://doi.org/10.1016/j.cirpj.2020.11.001
27. Baffari D, Reynolds AP, Li X, Fratini L (2017) Influence of processing parameters and initial temper on Friction Stir Extrusion of 2050 aluminum alloy. J Manuf Process 28:319–325. https://doi.org/10.1016/j.jmapro.2017.06.013
28. Shunmugasamy VC, Khalid E, Mansoor B (2021) Friction stir extrusion of ultra-thin wall biodegradable magnesium alloy tubes — microstructure and corrosion response. Mater Today Commun 26. https://doi.org/10.1016/j.mtcomm.2021.102129